Reading depth of the magnetic Barkhausen noise. II. Two-phase surface-treated steels.

A. Stupakov[a,*], A. Perevertov[a], M. Neslušan[b]

[a] *Institute of Physics of the Czech Academy of Sciences, Na Slovance 2, 18221 Prague, Czech Republic*

[b] *Faculty of Mechanical Engineering, University of Žilina, Univerzitná 1, 01026 Žilina, Slovakia*

Abstract

This second part of the work estimates the reading depth of the magnetic Barkhausen noise, testing surface-treated steels. The concomitant changes of the surface microstructure result in a pronounced two-peak profile of the Barkhausen noise signal: an additional peak arising from the surface-treated layer suppresses the initial peak generated in the bulk material. To confirm and explain the results obtained for semi-hard steel ribbons in the first part of this work [1], the steels with opposite surface treatments (soft decarburized and hard milled layers of different thickness) have been measured by commonly used detection sensors: classical sample-wrapping and industrial surface-mounted coils. To obtain physically accurate data, dynamic variations of the Barkhausen noise signal have been corrected using the recently proposed $\sqrt{dH/dt}$ normalization of its rms envelopes.

Keywords: Barkhausen noise, Surface sensitivity, Surface treatment

*Corresponding author. Tel: +420 26605 2114; E-mail: stupak@fzu.cz; URL: www.fzu.cz/˜stupak

1. Introduction

The first part of this work [1] has made a sole attempt to estimate the depth from which the Barkhausen noise (BN) signal is detected, testing martensitic steel ribbons of varied thickness. The technical problem of this straightforward approach are significant deviations of structural and magnetic properties of the ribbons with thickness caused by extensive rolling. Nevertheless, the rms intensity of the BN signal detected by classical sample-wrapping (encircling) coils [2, 3] saturates at an expected ribbon thickness ~ 200 μm. A similar dependence of the BN intensity obtained with industrial surface-mounted coils [4, 5] saturates at a lower ribbon thickness ~ 50 μm. Detailed analysis of the Fourier power spectra of BN signals explains this distinction in critical thickness level where the BN intensity saturates. In case of the surface-mounted coils, there is a significant loss of the BN intensity in the low-frequency part of the spectra.

In this second part of the work, we apply a commonly accepted method to estimate the BN reading depth. We have comprehensively tested two steel series with opposite surface treatments, resulting in soft decarburized and hard milled layers of varied thicknesses [6, 7]. To obtain physically accurate data, the surface-treated steels have first been measured by both commonly used types of the detection coils (sample-wrapping and surface-mounted) and a Hall sensor array to determine the sample magnetic field H [8]. A dynamic contribution to the BN signal has been eliminated using a proposed normalization of the BN rms profile (envelope) by a square root of the field rate of change, i.e. $U_{rms}(H)/\sqrt{dH/dt}$. The introduced square root term is explained by stochastic multiple overlapping of the independent BN pulses

[9].

Literature survey confirms a complexity of the studied problem: the obtained results are quite controversial. An overwhelming majority of the published papers has investigated an industrially attractive case of surface hardening. Such a surface layer, which is mechanically and magnetically harder, gives rise to an additional high-field peak on the BN envelopes. This second peak logically rises with thickness of the hardened surface layer at the expense of a suppressing main peak from the original steel bulk. Limit thickness value, at which the main BN peak vanishes, is usually taken to estimate the BN reading depth. Nowadays, the community's accepted value is about a few hundreds of micrometers [6, 10, 11]. However, this is a rather subtle compromise. Some researches [12, 13, 14, 15, 16] have proposed that the BN reading depth can reach up to 0.5–1 mm, even though the studied case hardened layers were quite inhomogeneous in depth. On the contrary, we have recently found that the main bulk peak of the BN envelope vanishes when thickness of the milled surface layer reaches only a few tens of micrometers [7].

2. Experimental

2.1. Materials

We have remeasured two available steel series with opposite types of surface treatments. The first series with softened surface layers was made from spring steel EN54SiCr6 of the following composition: 0.54% C, 0.68% Mn, 1.47% Si, 0.017% P, 0.009% S, 0.61% Cr, 0.05% Ni, 0.07% Cu and 0.032% Al. Plate-shaped samples with dimensions $110 \times 30 \times 3$ mm were annealed in

air at temperature 800°C for 0.5, 1, 4, 8 and 20 hours to induce a steel decarburization throughout whole plate surface. The soft surface layers consisting of a pure ferrite had $50 - 350$ μm thicknesses and 130–170 HV0.1 microhardness. Deeper transition layers consisting of a ferrite-pearlite mixture had $200 - 650$ μm thicknesses. The bulk pearlite steel had 260–300 HV0.1 kg microhardness. Non-magnetic surface oxides were removed by acid pickling. Reference samples without the decarburized layer, but with the similarly treated bulk, were annealed at the same conditions in a vacuum furnace. X-ray diffraction analysis proved a fine-grained polycrystalline structure and negligible tensile residual strains. There were two identical samples for each annealing time, which were measured from both sample sides for data averaging. More details can be found in the original work [6].

The second series with hardened surface layers was made from bearing steel 100Cr6 of the following composition: 0.98–1.1% C, 1.3–1.6% Cr, 0.25–0.45% Mn, 0.15–0.35% Si, S and P < 0.025%. It was austenitized at 840°C, quenched and tempered to a 50 ± 1 HRC hardness. One side of each sample was mechanically milled by cutting tools with a variable width of the flank wear land. This led to surface rehardening with a formation of so-called white layers of varied thicknesses in a range $0.7 - 11$ μm. The final samples of $70 \times 40 \times 4.5$ mm size were cut with the longest side along the axial milling direction. More details can be found in the original work [7].

2.2. Measurement

The steel plates were magnetized by U-shaped transformer yokes of the same length and width as the samples through a 1-mm air gap. The tangential components of the surface magnetic field were measured directly by

two Hall sensors at 1.5 and 2.7 mm above the yoke-free sample side. The magnetic field H in the samples was estimated by a linear extrapolation of these two measured tangential profiles to the sample surface [17]. The magnetizing frequency was low: $f_{mag} = 0.5$ Hz. The amplitudes of the magnetic field were fixed at $H_{max} = 4$ and 3 kA/m for the decarburized and the milled series, respectively. The measurements were performed in commonly used mode supplying the driving coils by the triangular magnetizing voltage $V(t)$, and in feedback mode attempting to adjust the magnetic field $H(t)$ to the triangular waveform [8]. The data are presented for the triangular $V(t)$ mode on default if it is not notified differently. Single sample-wrapping coils with 100 turns of wire detected the high-frequency BN as well as the low-frequency hysteresis signals: according to Faraday's law, the induced voltage $U_{ind} \propto dB/dt$, where B is magnetic induction. Our large surface-mounted coil, which photo is shown in Fig. 2(b) in [1], was also used for BN detection. The BN filtering bandwidth was 2–70 kHz for both detection coils. For each measurement, the envelope (rms profile) and the Fourier power spectrum of the BN signal were recorded. In addition to our previous works [6, 7], this work first compares the $\sqrt{dH/dt}$-normalized envelopes and the BN power spectra measured by both commonly used types of the detection coil. More details about the measurement procedure and the parameter evaluation methods can be found in the first part of this work [1].

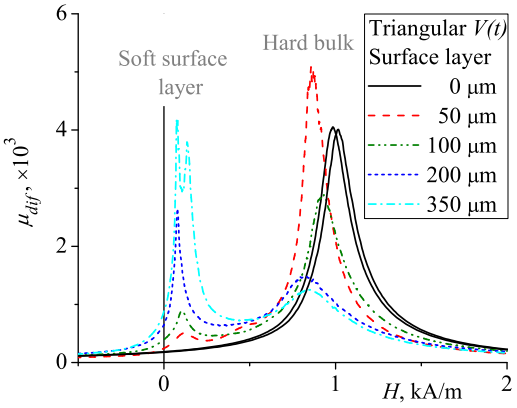

Figure 1: Ascending branches of the differential permeability curves $\mu_{dif} = dB/d(\mu_0 H)$ as functions of the magnetic field H measured at the triangular $V(t)$ for the decarburized steel series. The two black solid curves present the data obtained with the Hall sensors positioned at the opposite sides of the reference sample without the decarburized layer.

3. Results

3.1. Softened surface

Fig. 1 illustrates that the decarburized ferrite layers give clear low-field peaks even on the differential permeability curves $\mu_{dif}(H) = dB/d(\mu_0 H)$, where μ_0 is permeability of vacuum. It is worth noting that the permeability is detected from the whole sample cross-section. The first peak at $H \approx 80$ A/m is evident even for the thinnest ferrite layers of 50–100 μm thickness. For the surface layer of 200-μm thickness, the first peak starts prevailing over a high-field peak at $H \approx 850$ A/m accumulated from harder steel bulk. Areas under the separate permeability peaks correspond to fractions of the magnetic flux flowing through the two material phases [18]. Therefore, increase of the ferrite layer thickness leads to rise of the first permeability peak at the expense of the second one. The reference sample without the decarburized

layer produces a clear single peak at a slightly higher field $H \approx 1$ kA/m because it does not contain the transitional ferrite-pearlite zone. However, the surface field measurements of this reference sample from its opposite sides give slightly distant peaks caused by varied subsurface structures of rolled steel. For all decarburized samples, the two $\mu_{dif}(H)$ curves obtained with the side reversion are very similar. Therefore, only one such a curve for each layer thickness is shown in Fig. 1 for the sake of simplicity. Bifurcation of the low-field peak for the thickest 350-μm ferrite layer should be caused by inhomogeneous subsurface structure. The deeper transition layer consisting of a ferrite-pearlite mixture has a maximal thickness of 650 μm for this sample. The transition sublayer is slightly harder (mechanically and magnetically) than the surface ferrite layer. Therefore, such a thick transition sublayer can give rise to the second low-field peak at $H \approx 130$ A/m.

A varied structure of the reference sample on its opposite sides results in a double hump on the BN envelopes detected by sample-wrapping coil encircled along both sides (see Fig. 2). The BN envelopes for the sample with the thinnest 50-μm layer demonstrate two peaks of a comparable height. It is worth mentioning that the normalized envelopes in Fig. 2(b) demonstrate better peak separation and sharper low-field peaks, that are similar to the $\mu_{dif}(H)$ curves in Fig. 1, compared to the raw envelopes in Fig. 2(a). A humped profile of the normalized envelope in the field range $H = 300 - 900$ A/m for the sample with 100-μm layer confirms an existence of the transitional ferrite-pearlite zone. The normalized envelopes for the two last samples with 200/350-μm layers display not only the narrow peaks at $H \approx 80$ A/m but show distinguishable humps at $H \approx 750$ A/m.

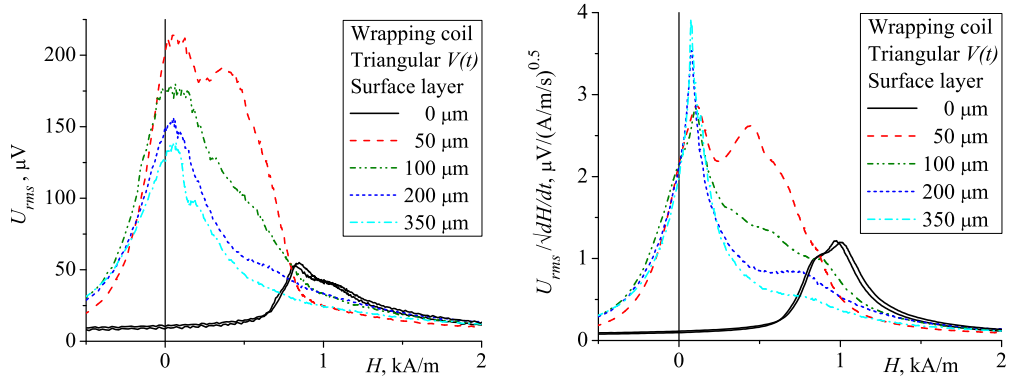

(a) (b)

Figure 2: Ascending branches of (a) the raw and (b) the corresponding $\sqrt{dH/dt}$-normalized envelopes of BN measured at the triangular $V(t)$ by sample-wrapping coil for decarburized steel series. The two black solid curves present the data obtained with the Hall sensors positioned at the opposite sides of the reference sample without the decarburized layer.

Appropriateness of the $\sqrt{dH/dt}$ envelope normalization is additionally illustrated by Fig. 3. The commonly used mode of the triangular magnetizing voltage $V(t)$ results in significant minimums of the field rates dH/dt at the positions of the μ_{dif} maximums as shown in Figs. 3(a)–(b). The dH/dt minimums guarantee a near quasi-static dc regime of magnetization at low frequencies $f_{mag} < 1$ Hz for ferritic steels. Our attempt to adjust the field waveform $H(t)$ to a triangular shape is not successful enough, but allows to perform the measurements at a higher dH/dt in a slightly dynamic regime [8]. This is evident from a dynamic decrease and high-field shift of the permeability peaks in Fig. 3(b) [19]. It is worth mentioning that the differential permeability is given by the low-frequency component of the voltage induced in sample-wrapping coil according to Faraday's law

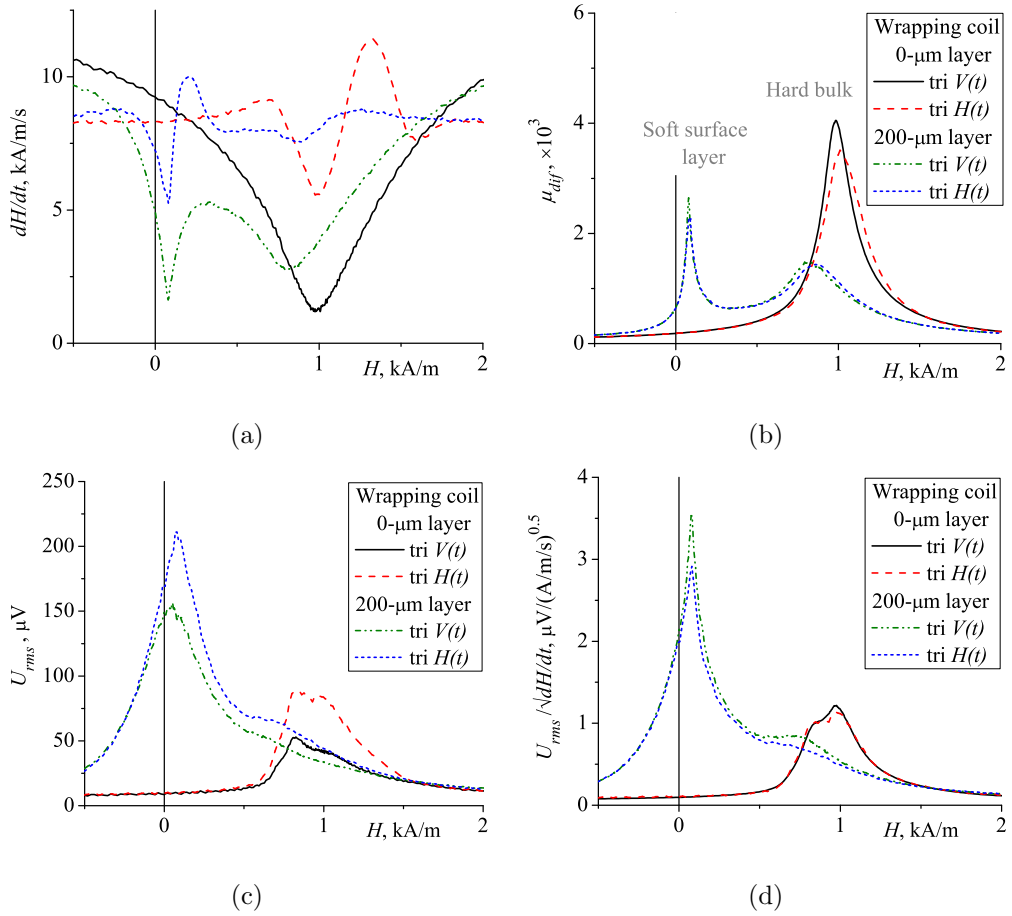

Figure 3: (a) Rates of change of the surface magnetic field $dH/dt(H)$ for the two samples with zero and 200-μm ferrite layers magnetized in both modes: triangular $V(t)$ and $H(t)$. The corresponding profiles of (b) the differential permeability $\mu_{dif}(H)$, (c) the raw and (d) the $\sqrt{dH/dt}$-normalized envelopes of BN measured by sample-wrapping coil.

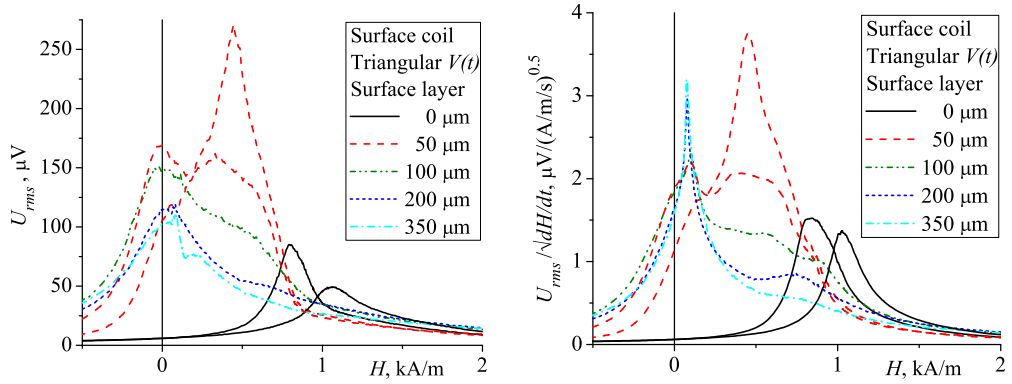

(a) (b)

Figure 4: Ascending branches of (a) the raw and (b) the corresponding $\sqrt{dH/dt}$-normalized envelopes of BN measured at the triangular $V(t)$ by surface-mounted coil for decarburized steel series. The two curves, black solid and red dashed, present the data obtained at the opposite sides of the two samples with zero and 50-μm layers, respectively.

$U_{ind} \propto dB/dt = \mu_0 \mu_{dif} dH/dt$, which is normalized by the field rate of change dH/dt [9]. The higher field rates dH/dt obtained at the triangular $H(t)$ mode elongate the corresponding raw envelopes as compared to those measured at the triangular $V(t)$ [see Fig. 3(c)]. The $\sqrt{dH/dt}$ normalization of these raw envelopes measured at different magnetizing rates makes them comparable. A small suppression of the peak heights for the higher dH/dt is in line with the dynamic behavior of the permeability [see Figs. 3(b) and 3(d)].

The measurements with the surface-mounted coil result in similar peak separation, although with slightly shorter first peaks (compare Figs. 2 and 4). The only significant difference is that the surface-mounted coil detects the BN signal locally from one sample side only: the reference sample without the decarburized layer and the sample with the thinnest 50-μm layer have distinct opposite sides. As it was mentioned above, different mechanical de-

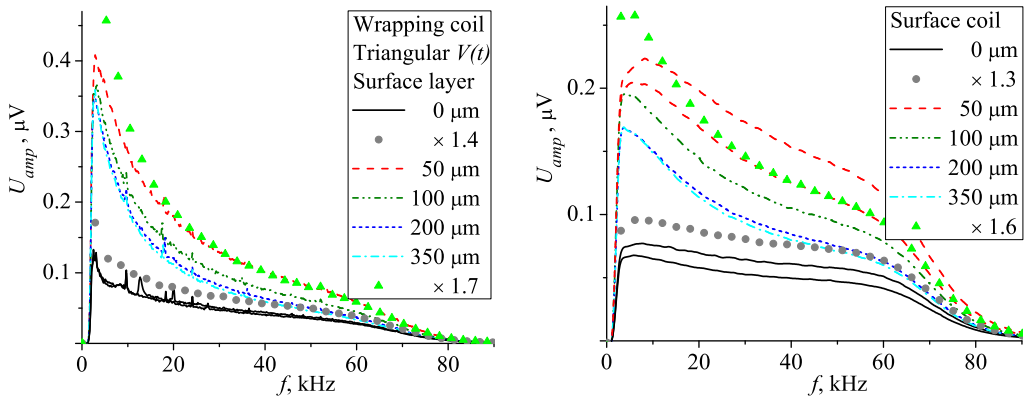

(a) (b)

Figure 5: Fourier power spectra of the BN signals measured at the triangular $V(t)$ for decarburized steel series by (a) sample-wrapping and (b) surface-mounted coils. The two black solid curves present the spectra obtained at the opposite sides of the reference sample to keep an analogy with Figs. 2 and 4. (b) The two red dashed curves keep a similar analogy with Fig. 4. The spectra for the samples with zero and 350-μm layers are additionally scaled [multiplied by 1.4/1.3 and 1.7/1.6 in (a)/(b) respectively] and shown by symbols for comparison with the spectra for the samples with 200-μm and 50-μm layers, respectively.

formation of the opposite steel surfaces during the rolling process can cause the observed difference in the BN signal for the reference sample. The sample bulk, however, is nearly homogenous as illustrated by the corresponding permeability curves in Fig. 1. Short annealing time applied for the sample with the thinnest 50-μm layer was probably not sufficient to remove the surface deformation to a necessary depth. For the rest of the decarburized samples, similar envelopes are obtained at both sides. The $\sqrt{dH/dt}$ normalization for the surface-mounted coil has identical influence on the envelopes than that shown in Fig. 3 for the sample-wrapping coil.

As already mentioned in the first part [1], the open sample-wrapping coil easily picks up the background noise resulting in visible parasitic harmonics on the power spectrum profiles [see Fig. 5(a)]. The spectra for the reference semi-hard sample without the decarburized layer have a small low-frequency peak at $f < 20$ kHz containing the long-lasting BN pulses. These long-lasting BN activity is more pronounced for decarburized samples with soft ferrite layers. Moreover, thicker ferrite layers intensify the low-f spectrum peaks. The same behavior is observed for the spectra detected by surface-mounted coil [see Fig. 5(b)]. However, the mentioned low-frequency peaks of BN power spectra detected by surface-mounted coil are less pronounced than those detected by sample-wrapping coil. For the reference semi-hard sample without the decarburized layer and the sample with the thinnest 50-μm layer, these low-f peaks are not noticeable at all.

Integration of the BN envelopes gives so-called BN loops similar to integration of the differential permeability curves to the hysteresis $B(H)$ loops. Intersection points of the obtained BN loops with the field axis allow to estimate the surface coercive field [6]. If the permeability curve or the BN envelope has a single-peak shape, the obtained coercive field is usually very close to the field position of the permeability/envelope peak. The BN H_c together with the hysteresis coercive field are shown in Fig. 6(a). Whereas the hysteresis H_c continuously decreases up to 460 A/m, the BN H_c falls down to 125 and 140 A/m at the ferrite layer thicknesses ~ 200 μm for the sample-wrapping and the surface-mounted coils, respectively. Realistic H_c value of the decarburized layers was obtained on a level of 94 A/m from the minor loop measurements with a low field amplitude $H_{max} = 300$ A/m when

only the soft surface layer was magnetized to saturation [17]. It agrees with the table data: for pure ferrite steel $H_c \approx 100$ A/m. Smaller values of the BN H_c obtained with sample-wrapping coil compared to those obtained with surface-mounted coil can be determined by different sensitivity in detection of the long-lasting BN pulses in the low-frequency part of the Fourier power spectra as shown in Fig. 5. On the other hand, the total number of the BN pulses that overcome a 20-μV threshold of background noise is up to 40% bigger for the surface-mounted than the sample-wrapping coil as shown in Fig. 6(b). The dependence of the BN counts on the decarburized layer thickness are nearly inverse to those of the BN H_c with a similar parameter saturation at the layer thicknesses ~ 200 μm.

3.2. Hardened surface

Fig. 7(a) presents the differential permeability curves for milled samples with hardened surface layers with an increased thickness up to 11 μm. For the layer thickness over 5 μm, the single peak profiles of the permeability slightly shift to higher fields. This shift is mostly caused by changes in the measured surface field because of a negligible volume of hardened fraction [see Fig. 7(b)]. The maximum permeability value $\sim$ 8 000 is rather high for construction steel, which causes a deep near-zero minimum of the dH/dt dependence. The tempered martensite matrix of the tested steel has preferable grain orientation along the magnetizing direction [20]. This favors simultaneous magnetization reversal inside the different magnetic domains and leads to a specific combination of high $\mu_{dif} \sim 10^4$ and a high $H_c > 1$ kA/m [21]. The positions of the permeability maximum correlate with those of the dH/dt minimum and is close to the coercive field $H_c \approx 1.4$ kA/m as

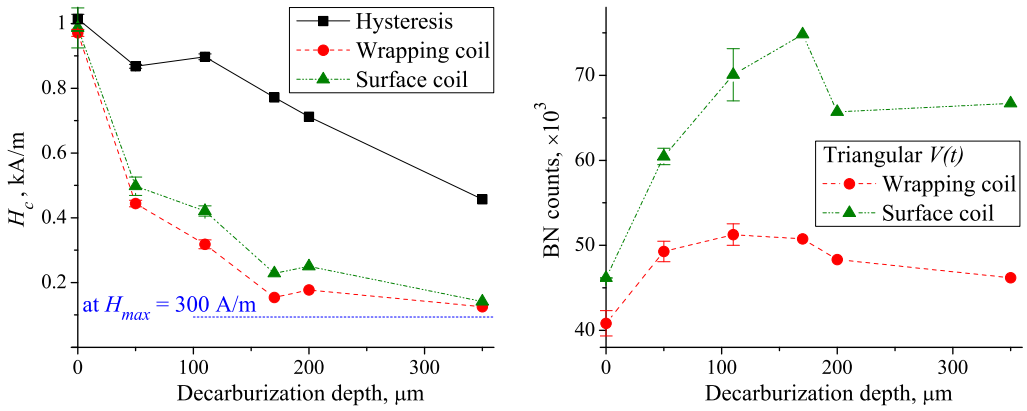

(a) (b)

Figure 6: (a) Coercive fields H_c evaluated from the hysteresis and the BN data for decarburized steel series. The measurements are performed at the triangular $V(t)$ by both detection coils. Coercivity 94 A/m of the decarburized ferrite layer estimated from the measurements at a low field amplitude H_{max} = 300 A/m is shown by the horizontal dashed line. (b) Corresponding number of the BN pulses over a 20-μV threshold. The error bars present the standard errors of the repeated tests including the measurements at the opposite sample sides.

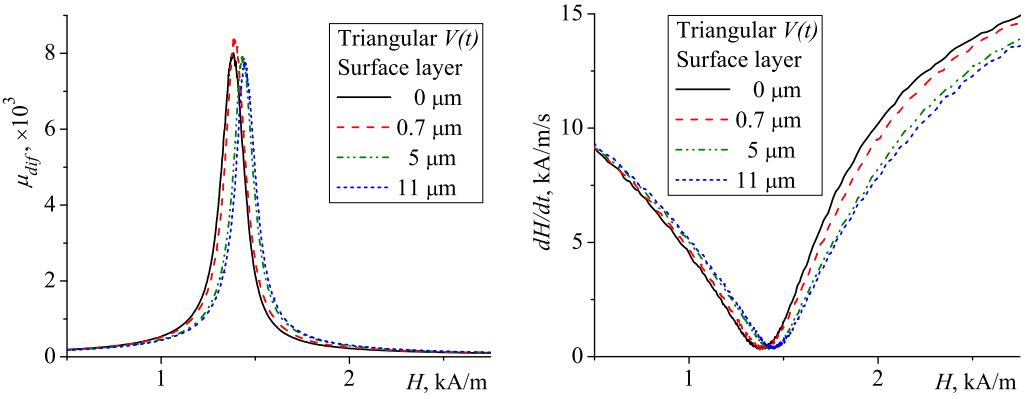

Figure 7: (a) Ascending branches of the differential permeability curves $\mu_{dif} = dB/d(\mu_0 H)$ as functions of the magnetic field H measured at the triangular $V(t)$ for milled steel series. (b) Corresponding rates of change of surface magnetic field $dH/dt(H)$.

explained above.

The steel bulk expectedly produces the permeability peaks as well as the first peaks of BN envelopes near the coercive field $H_c \approx 1.4$ kA/m, whereas the hardened surface layers give the second BN peak at a higher field $H \approx 1.8$ kA/m (see Figs. 8 and 9). However, the deep and wide minima of the dH/dt dependence shown in Fig. 7(b) evidently distort the raw BN envelopes. Even the raw envelopes for the bulk material measured at the unmilled surfaces have a two-peak shape, which transforms to an expected single-peak shape after the $\sqrt{dH/dt}$ normalization. The dH/dt minimum also suppresses the first bulk peak of the raw envelopes for the milled samples: this peak practically vanishes at the white layer thickness $\sim 5-11$ μm. However, the $\sqrt{dH/dt}$ normalization intensifies the suppressed first peaks. It is worth mentioning that the sample-wrapping coil detects the

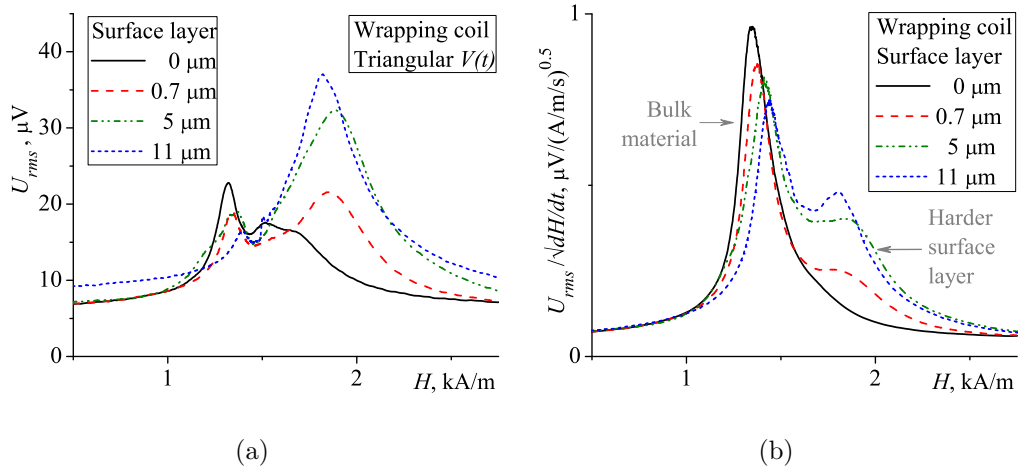

Figure 8: Ascending branches of (a) the raw and (b) the corresponding $\sqrt{dH/dt}$-normalized envelopes of BN measured at the triangular $V(t)$ by sample-wrapping coil for milled steel series.

BN signal from both sample sides: the tested milled as well as the opposite unmilled ones. Therefore, the corresponding first peak in Fig. 8(b) is nearly twice overrated. More reliable data obtained with the local surface-mounted coil give comparable heights of the two peaks for the white layer of 5-μm thickness. For the thickest 11-μm layer, the first bulk peak is still visible but already much lower than the second peak as illustrated by Fig. 9(b).

The Fourier power spectra of the BN signals detected by sample-wrapping coil contain significant spikes of parasitic noise harmonics as was mentioned above. The spectra profiles for the differently milled samples are identical, however the first low-f spike seems to be higher for the thickest white layer of 11 μm as shown in Fig. 10(a). The spectra obtained with the surface-mounted coil demonstrate a similar slight increase of the low-f peak with growing thickness of the white layer as shown in Fig. 10(b). In line with the

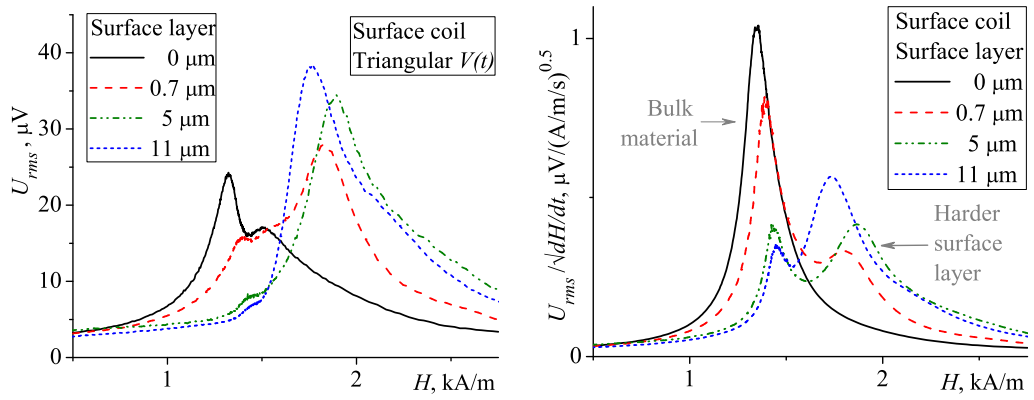

Figure 9: Ascending branches of (a) the raw and (b) the corresponding $\sqrt{dH/dt}$-normalized envelopes of BN measured at the triangular $V(t)$ by surface-mounted coil for milled steel series.

previous results, the spectrum profiles obtained with the surface-mounted coil are flatter than those obtained with the sample-wrapping coil.

The hysteresis and the BN coercive fields H_c measured by sample-wrapping coil demonstrate a small $\sim 50 - 100$ A/m rise for the white layer thickness > 2 μm. For the BN H_c measured by surface-mounted coil locally from the milled surface only, this rise is twice higher with an evident increase in a $5 - 11$ μm range as shown in Fig. 11(a). The total number of BN pulses does not change much in case of the detection by sample-wrapping coil from both sample sides. However, the pulse number significantly drops for local detection by surface-mounted coil as shown in Fig. 11(b). An inverse relation between the BN H_c and the count parameters is an expected trend: magnetically harder materials usually produce a fewer amount of BN pulses (see also Fig. 6).

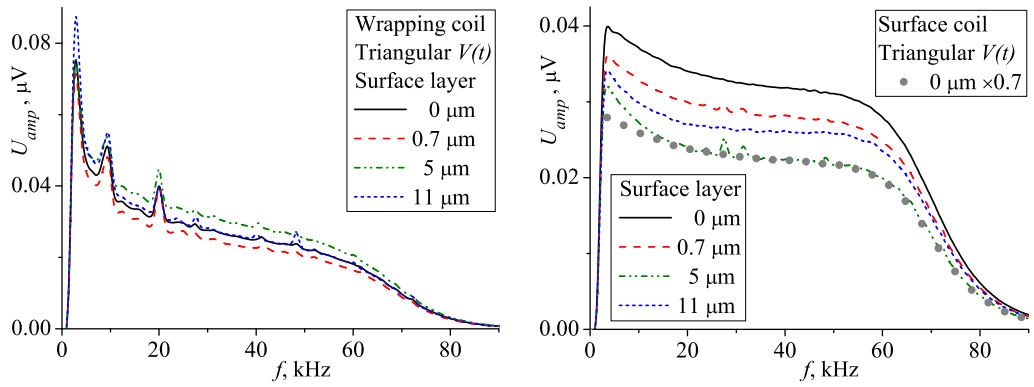

(a) (b)

Figure 10: Fourier power spectra of the BN signals measured at the triangular $V(t)$ for milled steel series by (a) sample-wrapping and (b) surface-mounted coils. (b) The spectrum for the unmilled sample is additionally scaled (multiplied by 0.7) and shown by symbols for comparison with the spectrum for sample with 5-μm layer.

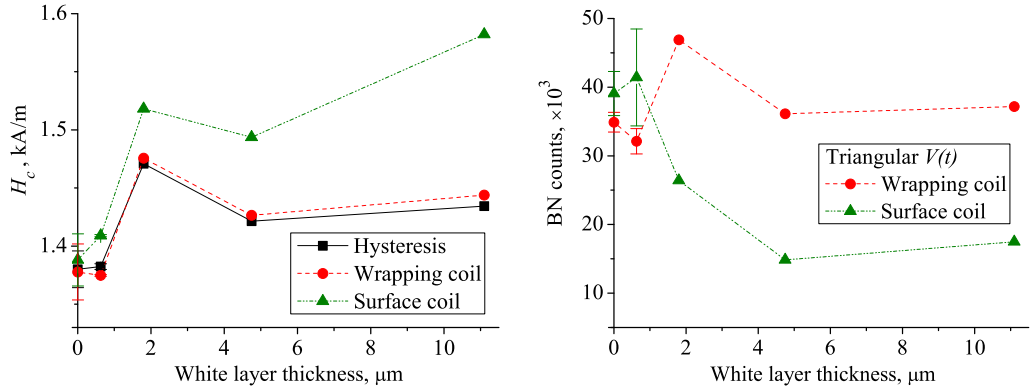

(a) (b)

Figure 11: (a) Coercive fields H_c evaluated from the hysteresis and the BN data for milled steel series. The measurements are performed at the triangular $V(t)$ by both detection coils. (b) Corresponding number of the BN pulses over a 20-μV threshold.

4. Discussion

The presented results give further evidence that accurate analysis of the two-peak BN envelopes obtained for two-phase surface-treated steels should be performed in terms of the $\sqrt{dH/dt}$-normalized profiles. This normalization transforms the envelope for the homogeneous one-phase material into the expected single-peak profile, as well as gives a pronounced two-peak profile with a continuous evolution of the peak heights in case of the two-phase surface-treated steels (see Figs. 2–4, 8 and 9) [9].

For the decarburized series with softened ferrite layers formed on the steel surface, comparable depth sensitivity of both detection coils is observed. The BN H_c falls significantly, up to the expected value of $\sim$ 100 A/m at layer thickness $\sim$ 200 μm for sample-wrapping as well as surface-mounted coils [see Fig. 6(a)]. A large size of ferrite grains $\sim$ 50 μm provides a logical explanation of this distinct result [6]. For the milled series, the first peak of the BN envelope from steel bulk detected by surface-mounted coil becomes minor at such a small thickness of harder white layer as $\sim$ 10 μm. Taking into account that the thickness of the subsurface transition layer should be of the same order, we can assume a total vanishing of this first bulk peak at a harder layer thickness $\sim$ 50 μm. This is exactly the level when the BN rms value detected by surface-mounted coil stops rising with increasing thickness of steel ribbons, as indicated in the first part of this work [1]. The milled steel and the ribbons, however, have much finer textures than the decarburized ferrite [7]. The fine structure can significantly complicate propagation of the BN pulses and distort the pulse overlapping pattern. A quantitative analysis of the overlapping mechanisms is hardly possible. The increasing amount of

BN pulses with thicker soft ferrite layers leads to a sharpening of the low-frequency part of the Fourier power spectra, which means a higher ratio of long-lasting pulses [see Figs. 5 and 6(b)]. However, it is difficult to explain the opposite trend observed for the milled series: a similar sharpening of the low-f spectra with a growing thickness of the hard white layer accompanied by a significant drop of the pulse count detected by surface-mounted coil [see Figs. 10(b) and 11(b)]. For instance, removing a significant part of the long-lasting pulses from the softer bulk material could ironically suppress the forming of longer-lasting overlapped pulses, which are cut off by the 2-kHz high-pass filter. This is because a period of the multiply overlapped final pulse can be much bigger than initial periods of the individual BN pulses. It is also worth mentioning that probability to be overlapped is higher for longer-lasting pulses. Therefore, we can arrive at the same conclusion as in the first part of this work [1]: the reading depth of the surface-mounted coil could be up to the same ~ 200 μm as in the case of sample-wrapping coil. However, the BN signal detected by surface-mounted coil seems to be more influenced and distorted by pulse overlapping than that detected by classical sample-wrapping coil.

Next interesting question is if variations of the bandpass filter frequencies could have an impact on the reading depth of BN. This question is closely related to a critical issue of a proper detection of the important low-frequency part of the BN signal (see Figs. 5 and 10). The frequency of the high-pass filter used in this work is by 2-4 times higher than those used in [10, 13, 14] but is by 4 times lower than that used in [11]. In case of the near-dc magnetizing rates $f_{mag} = 0.2 - 1$ Hz, the filter frequency cannot be smaller than $0.3 - 0.5$

kHz to get rid of the low-frequency Faraday signal properly [10, 14]. We did not reveal qualitative difference in the BN signal when the filter frequency was adjusted in a range $0.5-2$ kHz. Therefore, we commonly use the 2-kHz high-pass filter, which guarantees the stable and smooth BN envelopes/spectra without visible Faraday distortions. Decrease of the high-pass filter frequency below 0.3 kHz is possible only at lower magnetizing rates $f_{mag} < 0.1$ Hz, what significantly complicates the data acquisition and processing. In addition, increase of both cut-off frequencies of the bandpass filter did not reveal any significant influence on the BN reading depth [1, 7, 16].

Alongside with the above-made estimation of the reading depth, the obtained data underline controversial issues of the BN analysis. We still do not understand all details of the BN detection mechanism. In case of the surface-mounted coil, the situation is relatively clear: the coil picks up the magnetic impulses propagating perpendicular to the tested surface and the magnetizing direction into a space of the coil core. However, exact relations for the attenuation term [11, 22] and especially for the pulses overlapping [3, 23, 24] are still lacking. In case of the sample-wrapping coil, it is unclear why the coil does not pick up any considerable BN signal from the sample bulk similar to the low-frequency hysteresis response according to Faraday's law of induction [see Fig. 6(a)]. How is this bulk signal lost: is it suppressed by the dominating hysteresis component or eliminated due to pulse overlapping? Can a distorted flow of the micro eddy currents in the surface region be responsible for the bulk signal lost? Does the sample-wrapping coil detect only the parallel component of the magnetic pulses passing through the sample surface? Why do the two types of coils demonstrate different sensitivity

in the low-frequency part of the Fourier power spectra as shown in Figs. 5 and 10? These fundamental issues are still unanswered!

5. Conclusion

The presented results of testing the two-phase steels with opposite surface treatments are consistent with our previous data obtained from the martensitic steel ribbons of different thickness [1]. The measurements of a semi-hard steel with ferrite surface layers confirm that the reading depth of the magnetic Barkhausen noise detected by sample-wrapping as well as surface-mounted coils can reach ~ 200 μm for soft ferritic steels with large grains. For harder materials with fine structure, the Barkhausen noise signal detected by practical surface-mounted coil is significantly attenuated and distorted due to multiple overlapping of individual Barkhausen pulses, which is especially valid for long-lasting pulses. An effective reading depth (Barkhausen signal intensity) can thereby drop up to ~ 50 μm as in the studied cases of milled steel and martensitic ribbons. For these hard materials, the reading depth of classical sample-wrapping coil remains near the expected value of about 200 μm.

Acknowledgments

The work is supported by the Operational Programme Research, Development and Education financed by the European Structural and Investment Funds and the Czech Ministry of Education, Youth and Sports (Project No. SOLID21 - CZ.02.1.01/0.0/0.0/16_019/0000760) as well as by the VEGA

project No 1/0121/17. The authors thank Prof. B. Skrbek from the Technical University of Liberec for preparing the decarburized samples.

References

[1] A. Stupakov, A. Perevertov, M. Neslušan, Reading depth of the magnetic Barkhausen noise. I. One-phase semi-hard ribbons, J. Magn. Magn. Mater. 513 (2020) 167086 (12 pp), https://doi.org/10.1016/j.jmmm.2020.167086.

[2] R.M. Bozorth, J.F. Dillinger, Barkhausen effect. III. Nature of change of magnetization in elementary domains, Phys. Rev. 41 (1932) 345–355, https://doi.org/10.1103/PhysRev.41.345.

[3] G. Bertotti, F. Fiorillo, M.P. Sassi, Barkhausen noise and domain structure dynamics in Si-Fe at different points of the magnetization curve, J. Magn. Magn. Mater. 23 (1981) 136–148, https://doi.org/10.1016/0304-8853(81)90127-X.

[4] Yu Deng, Zhe Li, J. Chen, Xin Qi, The effects of the structure characteristics on magnetic Barkhausen noise in commercial steels, J. Magn. Magn. Mater. 451 (2018) 276–282, https://doi.org/10.1016/j.jmmm.2017.11.041.

[5] Y. He, M. Mehdi, E.J. Hilinski, A. Edrisy, Through-process characterization of local anisotropy of non-oriented electrical steel using magnetic Barkhausen noise, J. Magn. Magn. Mater. 453 (2018) 149–162, https://doi.org/10.1016/j.jmmm.2018.01.023.

[6] O. Stupakov, O. Perevertov, I. Tomáš, B. Skrbek, Evaluation of surface decarburization depth by magnetic Barkhausen noise technique, J. Magn. Magn. Mater. 323 (2011) 1692–1697, https://doi.org/10.1016/j.jmmm.2011.01.039.

[7] A. Stupakov, M. Neslušan, O. Perevertov, Detection of a milling-induced surface damage by the magnetic Barkhausen noise, J. Magn. Magn. Mater. 410 (2016) 198–209, https://doi.org/10.1016/j.jmmm.2016.03.036.

[8] A. Stupakov, O. Perevertov, V. Zablotskii, A system for controllable magnetic measurements of hysteresis and Barkhausen noise, IEEE Trans. Instrum. Measur. 65 (2016) 1087–1097, https://doi.org/10.1109/TIM.2015.2494621.

[9] A. Stupakov, Dynamic normalization of the Barkhausen noise signal, J. Magn. Magn. Mater. 482 (2019) 135–147, https://doi.org/10.1016/j.jmmm.2019.03.036.

[10] J.W. Wilson, G.Y. Tian, V. Moorthy, B.A. Shaw, Magneto-acoustic emission and magnetic Barkhausen emission for case depth measurement in En36 gear steel, IEEE Trans. Magn. 45 (2009) 177–183, https://doi.org/10.1109/TMAG.2008.2007537.

[11] A. Lasaosa, K. Gurruchaga, F. Arizti, A. Martínez-de-Guerenu, Quantitative estimation of nonmonotonic residual stress depth-profiles using an extended Kypris-Jiles model of the magnetic Barkhausen

noise spectrum, J. Appl. Phys. 123 (2018) 033904 (11 pp), https://doi.org/10.1063/1.5002074.

[12] M. Dubois, M. Fiset, Evaluation of case depth on steels by Barkhausen noise measurement, Mater. Sci. Technol. 11 (1995) 264–267, https://doi.org/10.1179/mst.1995.11.3.264.

[13] V. Moorthy, B.A. Shaw, P. Mountford, P. Hopkins, Magnetic Barkhausen emission technique for evaluation of residual stress alteration by grinding in case-carburised En36 steel, Acta Mater. 53 (2005) 4997–5006, https://doi.org/10.1016/j.actamat.2005.06.029.

[14] M. Blaow, J.T. Evans, B.A. Shaw, Effect of hardness and composition gradients on Barkhausen emission in case hardened steel, J. Magn. Magn. Mater. 303 (2006) 153–159, https://doi.org/10.1016/j.jmmm.2005.07.034.

[15] A. Lasaosa, K. Gurruchaga, F. Arizti, A. Martínez-de-Guerenu, Induction hardened layer characterization and grinding burn detection by magnetic Barkhausen noise analysis, J. Nondestruct. Eval. 36 (2017) 27 (7 pp), https://doi.org/10.1007/s10921-016-0388-y.

[16] A. Stupakov, R. Farda, M. Neslušan, A. Perevertov, T. Uchimoto, Evaluation of a nitrided case depth by the magnetic Barkhausen noise, J. Nondestruct. Eval. 36 (2017) 73 (9 pp), https://doi.org/10.1007/s10921-017-0452-2.

[17] O. Stupakov, Stabilization of Barkhausen noise readings by controlling

a surface field waveform, Measur. Sci. Technol. 25 (2014) 015604 (8 pp), https://doi.org/10.1088/0957-0233/25/1/015604.

[18] O. Perevertov, O. Stupakov, I. Tomáš, B. Skrbek, Detection of spring steel surface decarburization by magnetic hysteresis measurements, NDT&E Int. 44 (2011) 490–494, https://doi.org/10.1016/j.ndteint.2011.04.010.

[19] O.V. Perevertov, Application of the Preisach model to the magnetization process in steels, J. Phys. D: Appl. Phys. 35 (2002) 2467–2471, https://doi.org/10.1088/0022-3727/35/20/301.

[20] M. Neslušan, A. Mičietová, B. Hadzima, B. Mičieta, P. Kejzlar, J. Čapek, J. Uríček, F. Pastorek, Barkhausen noise emission in hard-milled surfaces, Materials 12 (2019) 660 (17 pp), https://doi.org/10.3390/ma12040660.

[21] O. Stupakov, Investigation of applicability of extrapolation method for sample field determination in single-yoke measuring setup, J. Magn. Magn. Mater. 307 (2006) 279–287, https://doi.org/10.1016/j.jmmm.2006.04.015.

[22] O. Kypris, I.C. Nlebedim, D.C. Jiles, Measuring stress variation with depth using Barkhausen signals, J. Magn. Magn. Mater. 407 (2016) 377–395, https://doi.org/10.1016/j.jmmm.2016.01.072.

[23] B. Ducharne, M.Q. Le, G. Sebald, P.J. Cottinet, D. Guyomar, Y. Hebrard, Characterization and modeling of magnetic domain wall dynamics using reconstituted hysteresis loops from

Barkhausen noise, J. Magn. Magn. Mater. 432 (2017) 231–238, https://doi.org/10.1016/j.jmmm.2017.01.096.

[24] Tu Le Manh, F. Caleyo, J.M. Hallen, J.H. Espina-Hernández, J.A. Pérez-Benitez, Model for the correlation between magnetocrystalline energy and Barkhausen noise in ferromagnetic materials, J. Magn. Magn. Mater. 454 (2018) 155–164, https://doi.org/10.1016/j.jmmm.2018.01.066.